

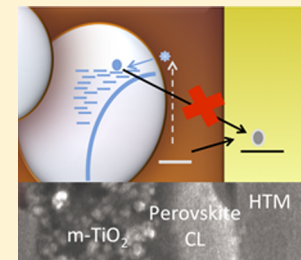
The Importance of Perovskite Pore Filling in Organometal Mixed Halide Sensitized TiO_2 -Based Solar Cells

Tomas Leijtens, Beat Lauber, Giles E. Eperon, Samuel D. Stranks, and Henry J. Snaith*

University of Oxford, Clarendon Laboratory, Parks Road, Oxford OX13PU, United Kingdom

 Supporting Information

ABSTRACT: Emerging from the field of dye-sensitized solar cells, organometal halide perovskite-based solar cells have recently attracted considerable attention. In these devices, the perovskite light absorbers can also be used as charge transporting materials, changing the requirements for efficient device architectures. The perovskite deposition can vary from merely sensitizing the TiO_2 electron transporting scaffold as an endowment of small nanoparticles, to completely filling the pores where it acts as both light absorber and hole transporting material in one. By decreasing the TiO_2 scaffold layer thickness, we change the solar cell architecture from perovskite-sensitized to completely perovskite-filled. We find that the latter case leads to improvements in device performance because higher electron densities can be sustained in the TiO_2 , improving electron transport rates and photovoltage. Importantly, the primary recombination pathway between the TiO_2 and the hole transporting material is blocked by the perovskite itself. This understanding helps to rationalize the high voltages attainable on mesoporous TiO_2 -based perovskite solar cells.



SECTION: Energy Conversion and Storage; Energy and Charge Transport

Initially developed by Graetzel and O'Regan in 1991, high efficiency dye-sensitized solar cells have long been considered as likely candidates for cheap, sustainable energy production.^{1,2} With the move from the corrosive liquid redox electrolytes to the solid state hole transporting material (HTM) spiro-MeOTAD,³ dye-sensitized solar cells appeared to be quickly becoming both efficient and stable.^{3,4} Solid-state dye-sensitized solar cells (ssDSSCs) have, however, fallen short of the predicted performances, reaching a maximum of 7.2% power conversion efficiency when using custom-synthesized light-absorbing dyes and specially designed dopants to improve the charge transport in the hole transporting layer.⁴ It was only recently, with organometal halide perovskites sensitizing the mesoporous TiO_2 electron-collecting anode, that solid-state sensitized solar cells have started to approach their predicted high performances. Following earlier work from Kojima et al.⁵ Kim et al. and Lee et al. demonstrated the use of $\text{CH}_3\text{NH}_3\text{PbI}_3$ and a "mixed halide" $\text{CH}_3\text{NH}_3\text{PbI}_{3-x}\text{Cl}_x$, respectively, in traditional solid-state dye-sensitized solar cell architectures.^{6,7} $\text{CH}_3\text{NH}_3\text{PbI}_{3-x}\text{Cl}_x$ has been shown to be capable of efficiently transporting charge carriers and hence can function in a "thin film" planar heterojunction solar cell configuration, while the $\text{CH}_3\text{NH}_3\text{PbI}_3$ perovskite was shown to be an effective hole transporter, negating the requirement to infiltrate the organic hole transporter, spiro-MeOTAD, into the TiO_2 mesopores.^{7–13} Indeed, the planar heterojunction solar cells have reached the highest performance to date of over 15% for the $\text{CH}_3\text{NH}_3\text{PbI}_{3-x}\text{Cl}_x$ perovskite.^{11–15} Moreover, some of the best results using $\text{CH}_3\text{NH}_3\text{PbI}_3$ come from device architectures where the perovskite deposition has been optimized to fill the TiO_2 mesopores and leave a capping layer of perovskite on top of the TiO_2 layer.^{16–18} The processes of charge transport and

recombination in such devices will necessarily differ from those in traditional ssDSSCs but, to the best of our knowledge, there has been no work on understanding the importance of perovskite filling of the mesoporous TiO_2 for device performance.

Here, we attempt to explain the differences in device performance observed when varying the degree to which the $\text{CH}_3\text{NH}_3\text{PbI}_{3-x}\text{Cl}_x$ perovskite fills the TiO_2 mesopores. By changing the TiO_2 layer thickness from 750 to 260 nm and changing the perovskite precursor spin coating solution concentration, we can gradually change the solar cell architecture from one where the perovskite truly acts as a sensitizer with nonuniform coverage, to one where the perovskite fills the majority of the pore volume uniformly and also acts as a hole transporter within the mesoporous two-component (TiO_2 and perovskite) composite.

In Figure 1, we show cross-sectional SEM images of the four different architectures used in this study, ranging from sensitized to completely perovskite-filled TiO_2 composites. We ensure a "sensitized" architecture (Figure 1a) by using a thick (750 nm) TiO_2 scaffold in conjunction with a low (30 wt %) concentration of perovskite precursor spin coating solution.⁷ Such films, however, do not absorb light very strongly, as shown in Figure 2a, so we have also used the same scaffold thickness in conjunction with a 40 wt % concentration of the perovskite precursor solution. In this case, we expect a higher coverage of the perovskite on the TiO_2 nanoparticles, but one that is still not continuous. These films then absorb

Received: January 29, 2014

Accepted: March 10, 2014

Published: March 10, 2014

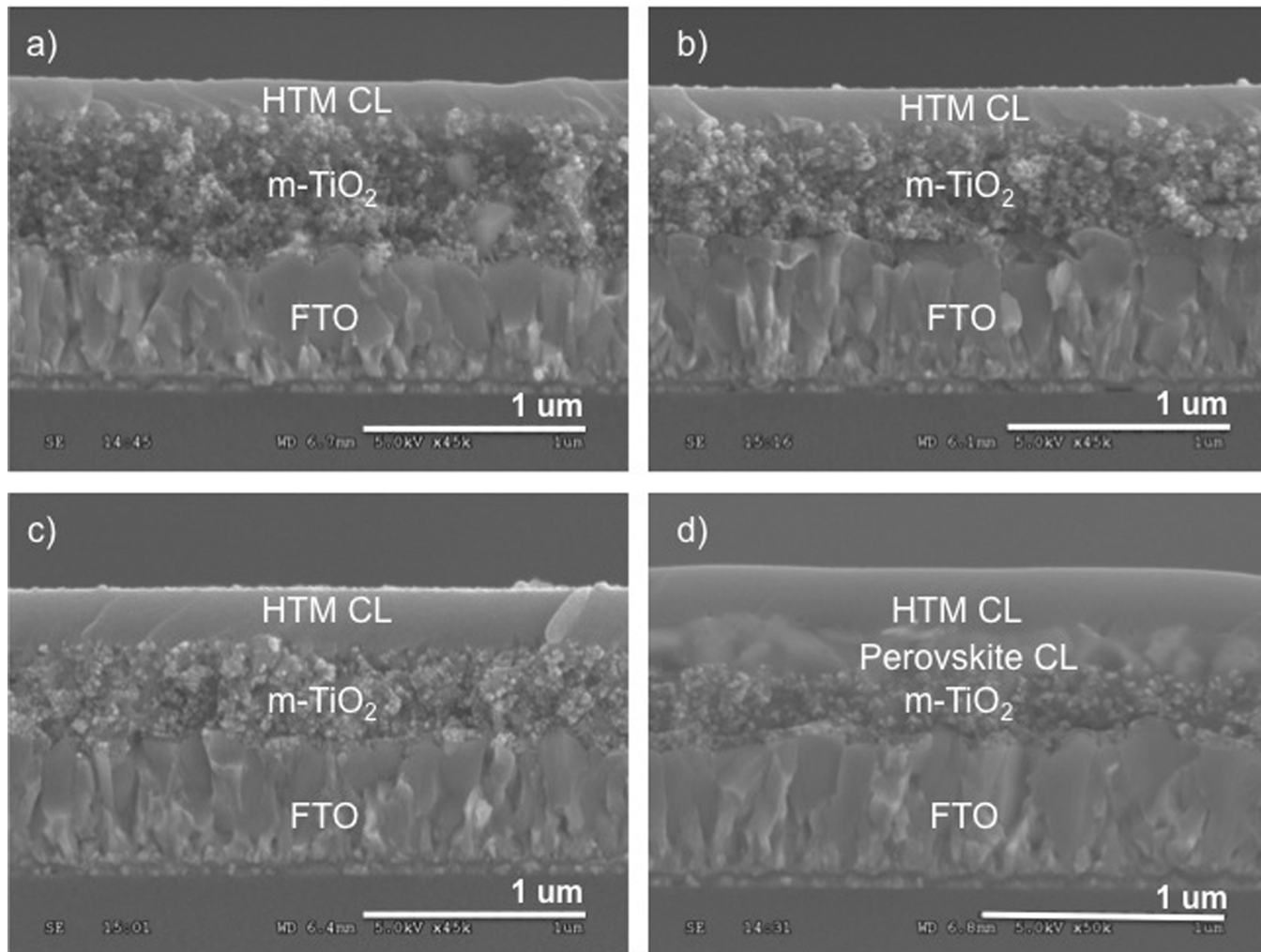


Figure 1. Device architectures. We depict cross-sectional SEM images of the different device architectures used, ranging from (a) a 750 nm TiO₂ scaffold (m-TiO₂) with 30 wt % perovskite precursor solution, to (b) 750 nm TiO₂ with 40 wt %, to (c) 440 nm TiO₂ with 40 wt %, to (d) 260 nm TiO₂ with 40 wt %. These architectures should correspond to changes from (a,b) sensitized with nonuniform coverage, to (c) predominantly perovskite-filled, to (d) fully perovskite filled with a perovskite capping layer (CL).

much more strongly, as seen in Figure 2a. To ensure a close to complete filling of the TiO₂ mesopores, we then decrease the scaffold thickness to 440 and 260 nm, as seen in Figure 1c,d respectively, while using a high 40 wt % precursor solution. Since capping layers of perovskite begin to form at TiO₂ scaffold thicknesses of just under 400 nm,⁸ it is at this thickness that we expect that we begin to completely, or close to completely, fill the pores of the TiO₂ with perovskite. Figure 1d clearly demonstrates the tendency of the perovskite to form a capping layer over the thin (260 nm) TiO₂ scaffold, so that we expect the perovskite pore filling to be high in such films.

We estimated the perovskite pore filling fractions by measuring the mass of large (31 cm²) substrates with the relevant TiO₂ layers before and after deposition of the mixed halide perovskite. Combined with knowledge of the unit cell size from XRD spectra (Figure S1) and hence density, we can estimate the total volume of the perovskite in the samples and hence the pore filling fractions. The results are presented in Table 1, while we give a full description of the calculations in the Supporting Information. The error in the calculation comes from consideration of the sensitivity of the scale, error in estimation of the substrate size, and error in determination of the size of the CH₃NH₃PbI_{3-x}Cl_x unit cell. The pore filling

fractions are evidently heavily dependent on the TiO₂ scaffold thickness, increasing from 47% in the thick TiO₂ scaffolds to around 100% with TiO₂ layers thinner than 400 nm. In the latter case, since there is negligible remaining porosity, the organic HTM spiro-MeOTAD is clearly unable to infiltrate the pores. Thus, the perovskite absorber must be transporting holes through the active layer to the p-type heterojunction.^{16,17} Where there is a perovskite capping layer, the perovskite must necessarily be capable of transporting both holes and electrons toward the mesoporous TiO₂.

In Figure 2b, we plot the current density vs voltage curves of the best solar cells with the architectures just described, while we present the extracted device performance parameters in Table 2. We also report the mean and standard deviation of each parameter for each device architecture in a given batch of devices. A description of the full statistical variation of a set of devices can be found in the Supporting Information (Figure S2). As the perovskite concentration increases and the scaffold thickness decreases (i.e., perovskite pore filling increases), we see a rapid improvement in both the photocurrent and photovoltages of the solar cells. We note that for the series using the same 40 wt % precursor solutions, the short-circuit currents rise quickly with decreased scaffold thickness, even

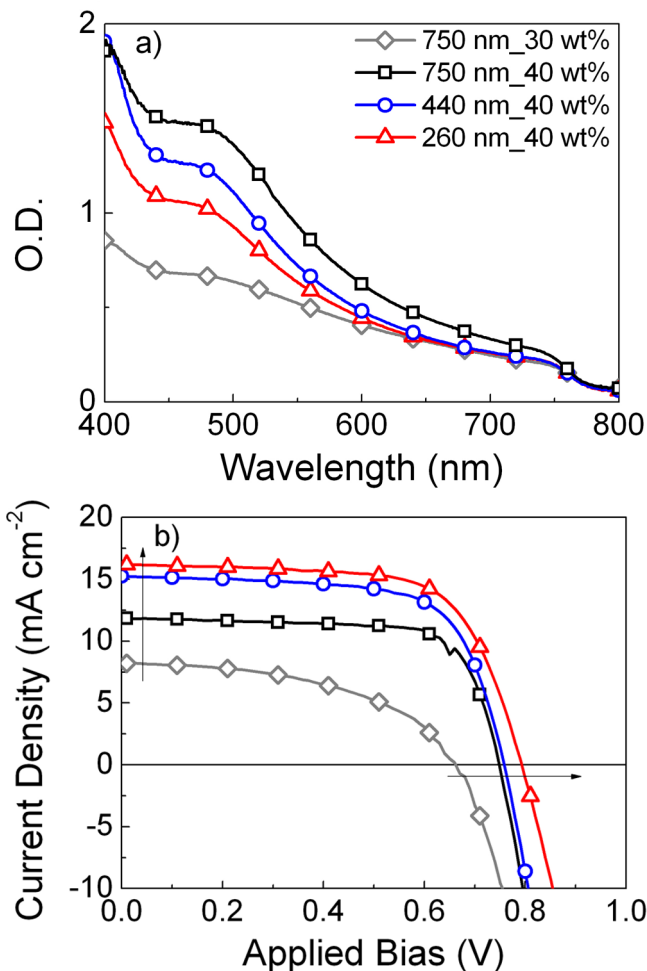


Figure 2. UV-vis spectroscopy and current density versus voltage curves of the solar cells. (a) UV-vis spectra of the relevant solar cells (before electrode deposition) with a 750 nm TiO₂ scaffold (m-TiO₂) with 30 wt % perovskite precursor solution (gray diamonds), 750 nm TiO₂ with 40 wt % (black squares), 440 nm TiO₂ with 40 wt % (blue circles), 260 nm TiO₂ with 40 wt % (red triangles). These were taken in transmission mode in an integrating sphere to account for scattering. (b) Current density versus voltage curves of the same solar cells measured under 100 mW cm⁻² simulated AM1.5 solar irradiation.

Table 1. Estimation of Perovskite Pore Filling and Coating Thickness

meso-TiO ₂ thickness	750 nm	750 nm	440 nm	260 nm
perovskite concentration	30 wt %	40 wt %	40 wt %	40 wt %
pore filling fraction (%)	47 ± 2	70 ± 3	108 ± 4	100 ± 5

though the optical density of the films is marginally decreased (Figure 2a). This means that the differences in photocurrent do not lie in light absorption, but rather in the charge collection efficiency. The greater than 100 mV improvement in photovoltage with decreased TiO₂ thickness could be expected if we consider that the electron density in the TiO₂ is increased, where the total charge generated is concentrated in a smaller volume of scaffold. This will lead to an increase in the electron quasi-Fermi level in the TiO₂, improving the photovoltage.^{19–21} The other possibility is that in devices with high perovskite pore filling, the charge actually resides in and is transported

through the perovskite itself, resulting in improved charge extraction and photovoltages.⁷

By employing quasi-steady state photoinduced absorption (PIA) spectroscopy (Figure 3), we aim to understand whether the improved photovoltage of the solar cells with thinner TiO₂ layers does indeed come from an increase in electron density within the TiO₂. By preparing samples identical to those used for the solar cells (but without spiro-MeOTAD or metal electrodes), we can monitor the electron density in each architecture under illumination. The PIA spectra of the different films used are plotted in figure 3, and all samples show a clear absorption peak centered around 1000 nm, which has been previously assigned to shallowly trapped electrons in TiO₂.²² We see this as evidence that even when the TiO₂ pores are largely filled with perovskite, electrons are transferred to the TiO₂ with a high efficiency, as was observed through photoluminescence decay studies of similar devices performed by Abrusci et al.²³ Recent time-resolved transient absorption measurements and impedance spectroscopy have also demonstrated this to be the case for the CH₃NH₃PbI₃ perovskite infiltrated into mesoporous TiO₂.^{24,25} When the photoinduced change in transmission is normalized for TiO₂ layer thickness and film O.D. at the laser excitation wavelength of 514 nm, we see that at a given generation rate, the electron density is indeed much higher in the thin TiO₂ layers than in the thicker layers. This is expected, since the thinner (260 nm) TiO₂ layers still have large capping layers of perovskite over significant portions of the active layer. Charges generated in the capping layer are rapidly transferred to the TiO₂ because of the high diffusivity of photogenerated carriers within the perovskite,¹¹ meaning that the total number of charges generated throughout the active layer are effectively concentrated into a thinner TiO₂ film.

We also expect the recombination rate to be slower. If we assumed the recombination is between electrons in the TiO₂ with holes in the perovskite, then there is simply less available surface area with the perovskite through which such recombination could occur. Reduced recombination rates would hence also contribute to an increased electron density in the thinner TiO₂ layers. It is then no surprise that the solar cells do depict significant improvements in photovoltage with decreasing TiO₂ thickness.

To probe the cause for improved photocurrents with decreased scaffold thicknesses, we perform small perturbation photocurrent and photovoltage decay measurements.²⁶ This technique allows us to probe the charge transport lifetimes as well as the short-circuit recombination lifetimes, the relative magnitudes of which can give an indication of the charge collection efficiency.²⁷ The results are depicted in Figure 4. We note that the charge transport lifetimes will be limited by the slow electron transport through the mesoporous TiO₂ at the relatively low charge densities found at short circuit.^{7,21,28} In Figure 4a, we plot the charge transport rates as a function of the background light intensity. Here, it is evident that at a given light intensity, the solar cells with thinner TiO₂ layers benefit from a decreased charge transport lifetime. If, however, the results are plotted as a function of the short-circuit electron density in TiO₂ (obtained through charge extraction measurements) as in Figure 4b, we can understand the reason for the aforementioned improved charge transport lifetimes. We see that the transport lifetimes in each architecture are very similar when compared at the same electron densities in the TiO₂. Moreover, the slopes of the lifetimes with electron density are also similar, demonstrating that regardless of device architec-

Table 2. Performance Parameters of the Best Devices with Different Perovskite Pore Filling Fractions^a

meso-TiO ₂ thickness	750 nm	750 nm	440 nm	260 nm
perovskite concentration	30 wt %	40 wt %	40 wt %	40 wt %
J_{sc} (mA cm ⁻²) (mean)	8.2	11.8	15.3	16.5
	6.3 ± 1.4	11.2 ± 2.0	13.6 ± 1.8	15.5 ± 1.3
PCE (%) (mean)	2.6	6.3	7.6	8.6
	1.9 ± 0.5	5.06 ± 1.2	6.3 ± 1.2	6.4 ± 1.6
V_{oc} (mean)	0.66	0.75	0.76	0.8
	0.67 ± 0.07	0.73 ± 0.03	0.74 ± 0.04	0.76 ± 0.05
FF (mean)	0.60	0.73	0.68	0.67
	0.49 ± 0.07	0.64 ± 0.08	0.62 ± 0.1	0.57 ± 0.1

^aWe present the mean values and the standard deviations for the batch of devices below the performance parameters of the highest performance solar cells.

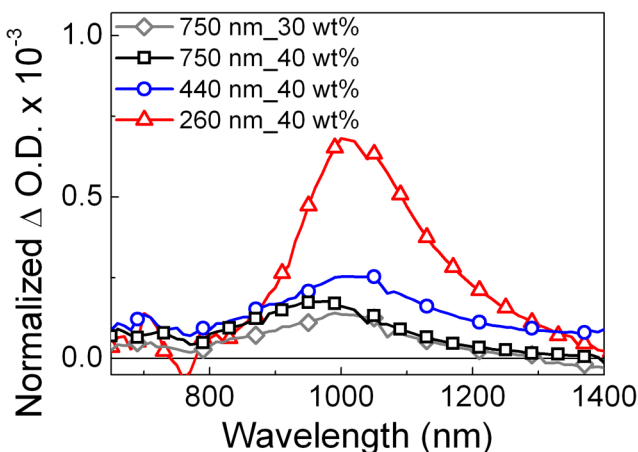


Figure 3. Photoinduced absorption spectroscopy of different architectures without HTM adjusted for generation rate. Quasi-steady-state photoinduced absorption spectra (PIA) were taken at an excitation wavelength of 514 nm and a fluence of 50 mW cm⁻², chopped at 23 Hz. We show the spectra for the relevant architectures: 750 nm TiO₂ scaffold with 30 wt % perovskite precursor solution (gray diamonds), 750 nm TiO₂ with 40 wt % (black squares), 440 nm TiO₂ with 40 wt % (blue circles), 260 nm TiO₂ with 40 wt % (red triangles). Samples did not contain any HTM in order for us to observe only the injected electron population. The data are normalized by device thickness and optical density at the excitation wavelength of 514 nm to adjust for differences in the generation rate.

ture, the electron transport is governed by the same multitrapping mechanism that has been widely accepted to be the mechanism for electron transport in mesoporous TiO₂.^{21,28–30} As we already observed in Figure 3, the thinner scaffolds simply build up higher charge densities in the TiO₂ at any given light intensity, and this leads to shorter charge transport lifetimes in the solar cells.

For the improved charge transport rates to translate to improved charge collection efficiencies, the short-circuit recombination in the thin solar cells must be significantly slower than the charge transport. In Figure 4c, we plot the short circuit recombination lifetimes as a function of charge density. It is immediately apparent that we can observe two distinctly different classes of behavior: we observe far steeper decreases in recombination lifetime with increasing charge density in the sensitized solar cells with thicker scaffolds, and hence low perovskite pore filling fractions, than in the solar cells with thinner scaffolds and higher perovskite pore filling. In fact, the short circuit recombination lifetimes for the thinner scaffolds are far slower, compared to those for the thicker scaffolds, at

the high charge densities that correspond to conditions under 1 sun. We see that the lifetimes for recombination ($\sim(2\text{--}3) \times 10^{-4}$ s) and transport ($\sim(2\text{--}3) \times 10^{-4}$ s) at high charge densities (one sun light intensity) are similar for the solar cells with low perovskite pore filling fractions, such that the collection is expected to be inefficient,²⁷ whereas the transport lifetimes ($\sim 6 \times 10^{-5}$ s) are significantly shorter than the recombination lifetimes ($\sim 3 \times 10^{-4}$ s) for the solar cells with highest perovskite pore filling fractions under the same light intensity.

Hence, we can confidently state that the solar cells made with thinner TiO₂ layers benefit from an improved charge collection efficiency. This appears to be because they can sustain high electron densities in the TiO₂, accelerating electron transport, without suffering from the rapid increase in recombination rates observed for the solar cells with lower perovskite coverage. In addition, a significant proportion of the electron migration across the active layer must take place within the solid perovskite film, prior to transporting to the mesoporous TiO₂. By comparing the slopes of electron transport lifetime with the electron density, we have also demonstrated that the electron transport mechanism responsible for the decay of the photocurrent remains the same, regardless of TiO₂ scaffold thickness, i.e., electrons are transported through the mesoporous TiO₂ to the collection electrode.

Perhaps the most interesting finding here is the decrease in the recombination rate's dependence on charge density, signifying a change in recombination mechanism. In the solar cells with low perovskite coverage, we expect the recombination mechanism to be similar to that found in dye sensitized solar cells, where electrons in the TiO₂ recombine with holes on spiro-OMeTAD.^{19,24,31} Since the coverage of perovskite is not expected to be completely uniform and there is likely to be some exposed TiO₂ allowing more unwanted contact with the spiro-OMeTAD, we might even expect the recombination to be faster than in solid state dye sensitized solar cells where the dyes form a dense layer on the TiO₂ surface. Indeed, the recombination lifetime of 3×10^{-4} s at a charge density of 10^{17} cm⁻³ observed here for sensitized cells is much faster than the 10^{-3} s or so observed at similar charge densities in solid state dye sensitized solar cells.^{24,31,32} We then propose the recombination mechanism depicted in Scheme 1a for the case where there is incomplete perovskite coverage on the mesoporous TiO₂. When the pores start to be completely filled with perovskite, the spiro-OMeTAD–TiO₂ contact will be virtually eliminated.¹⁶ Hence the primary recombination pathway will be largely removed, as displayed in Scheme 1b. Recombination of electrons in TiO₂ with holes in the

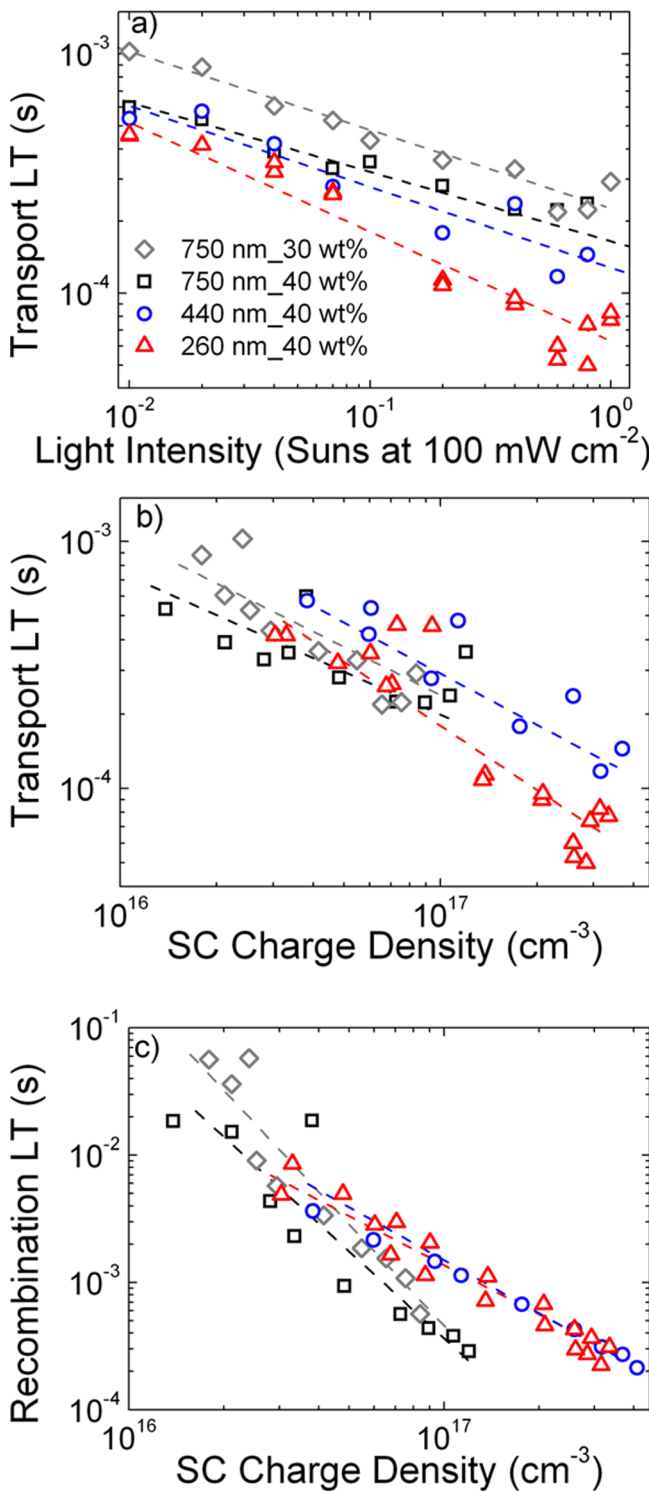
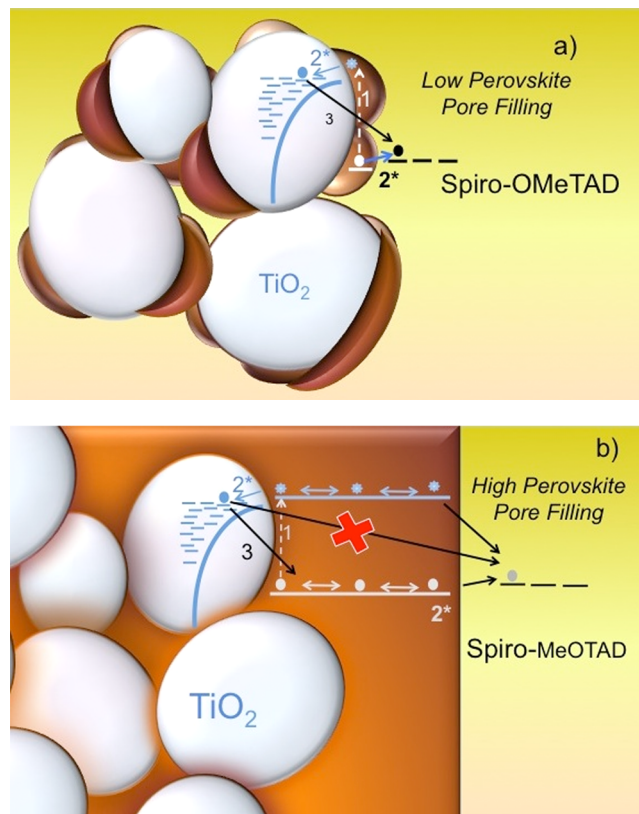


Figure 4. Transport and recombination lifetimes (LT). The transport lifetimes, obtained from small perturbation photocurrent decays, are plotted as a function of (a) light intensity and (b) charge density. (c) Recombination lifetimes at short circuit are plotted as a function of charge density. Gray diamonds correspond to the solar cells with 750 nm TiO_2 and 30 wt % perovskite precursor solution, while black squares are 750 nm TiO_2 with 40 wt % precursor solution, blue circles are 440 nm TiO_2 with 40 wt % precursor solution, and red triangles are 260 nm TiO_2 with 40 wt % perovskite precursor solution. The dotted lines are merely to guide the eye.

Scheme 1. Proposed Recombination Mechanisms for Solar Cells with Incomplete (a) and Complete (b) Perovskite Pore Filling Fractions^a



^aStep 1 (white arrow) stands for photo-excitation of the perovskite absorber, step 2 (light blue arrow) to electron injection into TiO_2 and hole transfer to the HTM, while step 3 (black arrows) represents the recombination pathways.

perovskite itself is moreover unlikely to be very fast, since the hole density in the perovskite should be relatively low due to their high diffusivity and effective transfer to spiro-OMeTAD at the planar heterojunction.¹¹ The same applies for the recombination of holes in spiro-OMeTAD with electrons in the perovskite: the electron density in the perovskite will be very low due to the fast electron transfer to the TiO_2 nanoparticles, meaning this recombination mechanism will also be very slow.²⁵

The understanding gained here allows us to propose design rules for preparing high efficiency TiO_2 -based perovskite solar cells. The most important factor to control is the completeness of perovskite coverage on the TiO_2 nanoparticles, as this reduces recombination rates. This means that higher charge densities can be maintained in the TiO_2 , improving the charge transport rates and collection efficiencies of the solar cells. This, together with the fact that thinner TiO_2 scaffolds serve to concentrate the electron density at a given generation rate, also leads to a raising of the electron quasi Fermi level in the TiO_2 to improve the photovoltage of the solar cells. In this work, we achieve this by reducing the TiO_2 scaffold thickness, which unfortunately decreases the optical density of the film. Future work is likely to be focused on using new deposition processes, such as the sequential deposition process introduced by Burschka et al.,¹⁸ to achieve high perovskite pore filling fractions with thicker active layers. Our work here also

emphasizes that the most efficient TiO_2 based perovskite solar cells operate in a distinctly different manner to conventional sensitized solar cells.¹⁶ The photogenerated electrons within the perovskite capping layer diffuse throughout this layer to the mesoporous TiO_2 electrode, and the holes throughout the whole of the photoactive layer are transported within the perovskite phase back to the planar heterojunction with the p-type hole-transporter. In essence, the mesoporous TiO_2 is performing the function of a rough electrode to facilitate long-lasting charge separation.

MATERIALS AND METHODS

The mixed halide perovskite ($\text{CH}_3\text{NH}_3\text{PbI}_{3-x}\text{Cl}_x$) precursor solution and solar cells were prepared as described previously.⁷ In short, fluorine-doped tin oxide coated glass substrates were cleaned sequentially in Hellmanex, acetone, isopropanol and oxygen plasma. A compact layer of TiO_2 (50 nm) was deposited by spin coating (2000 r.p.m., 2000 r.p.m s^{-1} ramp) a solution of titanium isopropoxide in ethanol (containing 35 μL of 2 M HCl per 5 mL of solution), and sintered at 500 °C for 30 min. The mesoporous TiO_2 layers were deposited by spin coating (2000 r.p.m., ramp 2000 r.p.m. s^{-1} for 60 s) solutions of commercial dyesol 18NR-T titania nanoparticle paste diluted at 1:2, 1:3, and 1:4 mass ratio of paste/ethanol to give 750 nm, 440 nm, and 260 nm films respectively. These films were then sintered in air at 500 °C for 45 min. The perovskite was deposited by spin coating (speed 2,000 r.p.m., ramp 2,000 r.p.m. s^{-1} , time 60 s) a 30 wt % or 40 wt % (as described in main text) DMF solution of methylammonium iodide and PbCl_2 (3:1 molar ratio). The substrate was then heated to 100 °C for 45 min in an oven in air. The hole-transport layer was deposited by spin coating 8.5 vol.% 2,2',7,7'-tetrakis(*N,N*-di-*p*-methoxyphenyl-amine)-9,9'-spirobifluorene (spiro-MeOTAD) in chlorobenzene with the standard additives tert-butylpyridine (0.80 mM) and lithium bis(trifluoromethanesulfonyl)imide (20 mM). Silver electrodes were then deposited by evaporation under high vacuum through a shadow mask.

For measuring the device performance parameters, Solar-simulated AM 1.5 sunlight was generated with an ABET solar simulator calibrated to give 100 mW cm^{-2} using an NREL-calibrated KG5 filtered silicon reference cell, and the JV curves were recorded with a sourcemeter (Keithley 2400, USA). The active area of the solar cells was defined by using a metal aperture mask of $\sim 0.09 \text{ cm}^2$.

Absorbance measurements of the films were taken with a commercial spectrophotometer (Varian Cary 300 UV-vis, USA) and an internally coupled integrating sphere (Labsphere, USA). An integrated photomultiplier tube detects the light inside the sphere. Samples were mounted at the entrance of the sphere, with a diffuse reflector mounted on an 8° wedge at the exit port.

Small Perturbation photovoltage and photocurrent decay measurements were performed as described elsewhere.^{26,32} Very briefly, an array of white light emitting diodes (LEDs) was used to change the background light intensity, and red LEDs were used to add a small (<10%) perturbation on top of this background. The change in photocurrent and photovoltage were recorded by an oscilloscope. For the recombination lifetime at short circuit, the cell was held at the short circuit current induced by the background light intensity, so that the red LED perturbation affected only the voltage of the cell, the decay of which allows us to estimate the recombination rate constants.

For the photoinduced absorption experiment, a continuous, tunable, Argon ion laser was used at a laser fluence of 50 mW cm^{-2} with an excitation wavelength of 514 nm and a modulation frequency of 23 Hz. A lock-in amplifier was used to detect the modulation of the light transmission, and was referenced to the modulation frequency. A 100 W halogen lamp was used as the white light probe, and the light monochromated after it had passed the sample. Here, the samples used were identical to the solar cells except that no spiro-MeOTAD or electrodes were used to allow us to detect the change in electron population in the TiO_2 .

ASSOCIATED CONTENT

Supporting Information

Description of pore filling calculations and solar cell performance statistics. This material is available free of charge via the Internet at <http://pubs.acs.org>.

AUTHOR INFORMATION

Corresponding Author

*E-mail: h.snaith1@physics.ox.ac.uk.

Notes

The authors declare no competing financial interest.

ACKNOWLEDGMENTS

The research leading to these results has received funding from the European Union Seventh Framework Programme [FP7/2007-2013] under grant agreement 316494 and the HYPER Project. G.E.E. is supported by Oxford Photovoltaics, Ltd. through a Nanotechnology KTN CASE award.

REFERENCES

- O'Regan, B.; Grätzel, M. A Low-Cost, High-Efficiency Solar Cell Based on Dye-Sensitized Colloidal TiO_2 Films. *Nature* **1991**, *353*, 737–740.
- Yella, A.; Lee, H.-W.; Tsao, H. N.; Yi, C.; Chandiran, A. K.; Nazeeruddin, M. K.; Diau, E. W.-G.; Yeh, C.-Y.; Zakeeruddin, S. M.; Grätzel, M. Porphyrin-Sensitized Solar Cells with Cobalt (II/III)-Based Redox Electrolyte Exceed 12% Efficiency. *Science* **2011**, *334*, 629–634.
- Bach, U.; Lupo, D.; Comte, P.; Moser, J. E.; Weissortel, F.; Salbeck, J.; Spreitzer, H.; Grätzel, M. Solid-State Dye-Sensitized Mesoporous TiO_2 Solar Cells with High Photon-to-Electron Conversion Efficiencies. *Nature* **1998**, *395*, 583–585.
- Burschka, J.; Dualeh, A.; Kessler, F.; Baranoff, E.; Cevey-Ha, N.-L.; Yi, C.; Nazeeruddin, M. K.; Grätzel, M. Tris(2-(1H-pyrazol-1-yl)pyridine)cobalt(III) as P-Type Dopant for Organic Semiconductors and Its Application in Highly Efficient Solid-State Dye-Sensitized Solar Cells. *J. Am. Chem. Soc.* **2011**, *133*, 18042–18045.
- Kojima, A.; Teshima, K.; Shirai, Y.; Miyasaka, T. Organometal Halide Perovskites as Visible-Light Sensitizers for Photovoltaic Cells. *J. Am. Chem. Soc.* **2009**, *131*, 6050–6051.
- Kim, H.-S.; Lee, C.-R.; Im, J.-H.; Lee, K.-B.; Moehl, T.; Marchioro, A.; Moon, S.-J.; Humphry-Baker, R.; Yum, J.-H.; Moser, J. E.; et al. Lead Iodide Perovskite Sensitized All-Solid-State Submicron Thin Film Mesoscopic Solar Cell with Efficiency Exceeding 9%. *Sci. Rep.* **2012**, *2*.
- Lee, M. M.; Teuscher, J.; Miyasaka, T.; Murakami, T. N.; Snaith, H. J. Efficient Hybrid Solar Cells Based on Meso-Superstructured Organometal Halide Perovskites. *Science* **2012**, *338*, 643–647.
- Ball, J. M.; Lee, M. M.; Hey, A.; Snaith, H. J. Low-Temperature Processed Meso-Superstructured to Thin-Film Perovskite Solar Cells. *Energy Environ. Sci.* **2013**, *6*, 1739–1743.
- Etgari, L.; Gao, P.; Xue, Z.; Peng, Q.; Chandiran, A. K.; Liu, B.; Nazeeruddin, M. K.; Grätzel, M. Mesoscopic $\text{CH}_3\text{NH}_3\text{PbI}_3/\text{TiO}_2$

- Heterojunction Solar Cells. *J. Am. Chem. Soc.* **2012**, *134*, 17396–17399.
- (10) Laban, W. A.; Etgar, L. Depleted Hole Conductor-Free Lead Halide Iodide Heterojunction Solar Cells. *Energy Environ. Sci.* **2013**, *6*, 3249–3253.
- (11) Stranks, S. D.; Eperon, G. E.; Grancini, G.; Menelaou, C.; Alcocer, M. J. P.; Leijtens, T.; Herz, L. M.; Petrozza, A.; Snaith, H. J. Electron-Hole Diffusion Lengths Exceeding 1 Micrometer in an Organometal Trihalide Perovskite Absorber. *Science* **2013**, *342*, 341–344.
- (12) Eperon, G. E.; Burlakov, V. M.; Docampo, P.; Goriely, A.; Snaith, H. J. Morphological Control for High Performance, Solution-Processed Planar Heterojunction Perovskite Solar Cells. *Adv. Funct. Mater.* **2013**, *24*, 151–157.
- (13) Liu, M.; Johnston, M. B.; Snaith, H. J. Efficient Planar Heterojunction Perovskite Solar Cells by Vapour Deposition. *Nature* **2013**, *501*, 395–398.
- (14) Docampo, P.; Ball, J. M.; Darwich, M.; Eperon, G. E.; Snaith, H. J. Efficient Organometal Trihalide Perovskite Planar-Heterojunction Solar Cells on Flexible Polymer Substrates. *Nat. Commun.* **2013**, *4*, 2761.
- (15) Jeng, J.-Y.; Chiang, Y.-F.; Lee, M.-H.; Peng, S.-R.; Guo, T.-F.; Chen, P.; Wen, T.-C. $\text{CH}_3\text{NH}_3\text{PbI}_3$ Perovskite/Fullerene Planar-Heterojunction Hybrid Solar Cells. *Adv. Mater.* **2013**, *25*, 3727–3732.
- (16) Heo, J. H.; Im, S. H.; Noh, J. H.; Mandal, T. N.; Lim, C.-S.; Chang, J. A.; Lee, Y. H.; Kim, H.; Sarkar, A.; NazeeruddinMd, K.; et al. Efficient Inorganic–Organic Hybrid Heterojunction Solar Cells Containing Perovskite Compound and Polymeric Hole Conductors. *Nat. Photonics* **2013**, *7*, 486–491.
- (17) Noh, J. H.; Im, S. H.; Heo, J. H.; Mandal, T. N.; Seok, S., II. Chemical Management for Colorful, Efficient, and Stable Inorganic–Organic Hybrid Nanostructured Solar Cells. *Nano Lett.* **2013**, *13*, 1764–1769.
- (18) Burschka, J.; Pellet, N.; Moon, S.-J.; Humphry-Baker, R.; Gao, P.; Nazeeruddin, M. K.; Grätzel, M. Sequential Deposition as a Route to High-Performance Perovskite-Sensitized Solar Cells. *Nature* **2013**, *499*, 316–319.
- (19) Fabregat-Santiago, F.; Bisquert, J.; Cevey, L.; Chen, P.; Wang, M.; Zakeeruddin, S. M.; Grätzel, M. Electron Transport and Recombination in Solid-State Dye Solar Cell with Spiro-OMeTAD as Hole Conductor. *J. Am. Chem. Soc.* **2008**, *131*, 558–562.
- (20) Snaith, H. J. Estimating the Maximum Attainable Efficiency in Dye-Sensitized Solar Cells. *Adv. Funct. Mater.* **2010**, *20*, 13–19.
- (21) Leijtens, T.; Lim, J.; Teuscher, J.; Park, T.; Snaith, H. J. Charge Density Dependent Mobility of Organic Hole-Transporters and Mesoporous TiO_2 Determined by Transient Mobility Spectroscopy: Implications to Dye-Sensitized and Organic Solar Cells. *Adv. Mater.* **2013**, *25*, 3227–3233.
- (22) Anderson, A. Y.; Barnes, P. R. F.; Durrant, J. R.; O'Regan, B. C. Simultaneous Transient Absorption and Transient Electrical Measurements on Operating Dye-Sensitized Solar Cells: Elucidating the Intermediates in Iodide Oxidation. *J. Phys. Chem. C* **2010**, *114*, 1953–1958.
- (23) Abrusci, A.; Stranks, S. D.; Docampo, P.; Yip, H.-L.; Jen, A. K. Y.; Snaith, H. J. High-Performance Perovskite–Polymer Hybrid Solar Cells via Electronic Coupling with Fullerene Monolayers. *Nano Lett.* **2013**, *13*, 3124–3128.
- (24) Zhao, Y.; Nardes, A. M.; Zhu, K. Solid-State Mesostructured Perovskite $\text{CH}_3\text{NH}_3\text{PbI}_3$ Solar Cells: Charge Transport, Recombination, and Diffusion Length. *J. Phys. Chem. Lett.* **2014**, *490*–494.
- (25) Marchioro, A.; Teuscher, J.; Friedrich, D.; Kunst, M.; van de Krol, R.; Moehl, T.; Grätzel, M.; Moser, J.-E. Unravelling the Mechanism of Photoinduced Charge Transfer Processes in Lead Iodide Perovskite Solar Cells. *Nat. Photonics* **2014**, *8*, 250–255.
- (26) O'Regan, B. C.; Lenzmann, F. Charge Transport and Recombination in a Nanoscale Interpenetrating Network of N-Type and P-Type Semiconductors: Transient Photocurrent and Photovoltage Studies of $\text{TiO}_2/\text{Dye}/\text{CuSCN}$ Photovoltaic Cells. *J. Phys. Chem. B* **2004**, *108*, 4342–4350.
- (27) Sivaram, V.; Kirkpatrick, J.; Snaith, H. Critique of Charge Collection Efficiencies Calculated through Small Perturbation Measurements of Dye Sensitized Solar Cells. *J. Appl. Phys.* **2013**, *113*, 063709.
- (28) Kopidakis, N.; Benkstein, K. D.; van de Lagemaat, J.; Frank, A. J. Transport-Limited Recombination of Photocarriers in Dye-Sensitized Nanocrystalline TiO_2 Solar Cells. *J. Phys. Chem. B* **2003**, *107*, 11307–11315.
- (29) Docampo, P.; Gulden, S. Charge Transport Limitations in Self-Assembled TiO_2 Photoanodes for Dye-Sensitized Solar Cells. *J. Phys. Chem. Lett.* **2013**, *4*, 698–703.
- (30) van de Lagemaat, J.; Frank, A. J. Nonthermalized Electron Transport in Dye-Sensitized Nanocrystalline TiO_2 Films: Transient Photocurrent and Random-Walk Modeling Studies. *J. Phys. Chem. B* **2001**, *105*, 11194–11205.
- (31) Kruger, J.; Plass, R.; Cevey, L.; Piccirelli, M.; Grätzel, M.; Bach, U. High Efficiency Solid-State Photovoltaic Device Due to Inhibition of Interface Charge Recombination. *Appl. Phys. Lett.* **2001**, *79*, 2085–2087.
- (32) Abate, A.; Leijtens, T.; Pathak, S.; Teuscher, J.; Avolio, R.; Errico, M. E.; Kirkpatrick, J.; Ball, J. M.; Docampo, P.; McPherson, I.; et al. Lithium Salts as “Redox Active” P-Type Dopants for Organic Semiconductors and Their Impact in Solid-State Dye-Sensitized Solar Cells. *Phys. Chem. Chem. Phys.* **2013**, *15*, 2572–2579.